scientific reports

Check for updates

OPEN

aFGF rescues high glucose-induced senescent fibroblasts and improves diabetic wound healing by regulating SIRT1/STAT3 pathway

Xiaoyang Wang[1,2,3,4], Meiqi Lu[1,2,3,4], Shanshan Jia[1,2,3], Jingjuan Zhang[1,2,3], Xiao Wang[2], Yongjun Qi[2], Nian Shi[1,2,3], Ya Jiao[3], Jie Zhao[3]✉, Xiaochuan Wang[2]✉, Jixun Zhang[2]✉ & Duyin Jiang[1,2,3]✉

In the wound of diabetic patients, Fibroblasts are extensively senescent and dysfunctional, resulting in prolonged skin wound healing time. The aim of this study was to investigate the impact of aFGF on diabetic wound healing and the senescence of fibroblasts induced by high glucose, and to explore the underlying mechanisms. We injected aFGF locally into the back wound of (Streptozocin) STZ-induced diabetic rats, and subsequently assessed its therapeutic impact on wound healing in vivo by measuring the wound healing rate and the expression of aging markers. Next, we conducted a series of in vitro experiments utilizing HG-induced L929 fibroblasts to evaluate the effects of aFGF on their aging and modulation of oxidative stress. Finally, we evaluated the changes of SIRT1 expression levels and phosphorylation STAT3 (Y705) levels, and observed whether the therapeutic effect of aFGF on diabetic wounds is related to the regulation of this pathway. Local injection of aFGF into diabetic wounds accelerates wound closure and decreases senescence associated secretory phenotype (SASP) expression. In vitro, aFGF enhanced the anti-senescence and antioxidant capacity of HG-induced senescent fibroblasts. It was found that aFGF effectively rescued SIRT1 expression and inhibited STAT3 phosphorylation in senescent tissue of diabetic wound. Our findings suggested that aFGF ameliorates the dysfunction of senescent fibroblasts by modulating the SIRT1/STAT3 signaling axis, thereby accelerating diabetic wound healing. aFGF is a promising therapeutic candidate for the treatment of diabetic wounds.

Keywords Acidic fibroblast growth factor, Diabetic wounds, Fibroblast, Senescence, SASP

In recent years, with the rapidly increasing number of people suffering from diabetes mellitus (DM), diabetic ulcers have become one of the most intractable problems in human health[1,2]. As a prevalent disease caused by disorders of glucose metabolism, DM is characterised by hyperglycemia and the irreversible formation and accumulation of advanced glycosylation end products (AGEs). Hyperglycemia expedites the formation of AGEs at the same time, and AGEs is an important feature of aging tissue[3,4]. It is well acknowledged that these factors actively contribute to the development and pathological healing in the diabetic wound characterized by senescence of fibroblasts, degradation of extracellular matrix (ECM) and locally increased inflammatory reaction[5–8]. Among these pathological features, fibroblast senescence stands out as a core driver of delayed diabetic wound healing. Senescent fibroblasts not only lose the ability to proliferate and synthesize key ECM components but also secrete a large number of senescence-associated secretory phenotype (SASP) factors. These factors inhibit the function of adjacent normal fibroblasts and aggravate local chronic inflammation, forming a "senescence-inflammation" vicious cycle that hinders wound repair[8,9]. Therefore, targeting fibroblast senescence-related pathways can significantly promote diabetic wound healing[10].

Sirtuins are a family of proteins implicated in a variety of cellular functions related to cell cycle, senescence, inflammation, cell proliferation and so on[11]. Among which, SIRT1 is a highly conserved NAD-dependent

[1]The Second Hospital of Shandong University, Jinan 250033, Shandong, China. [2]Department of Burns and Plastic Surgery, The Second Hospital of Shandong University, Jinan 250033, Shandong, China. [3]Department of Emergency, The Second Hospital of Shandong University, Jinan 250033, China. [4]Xiaoyang Wang and Meiqi Lu are co-first authors of the article. ✉email: 420458387@qq.com; xiaochuanbest@163.com; 200662011915@mail.sdu.edu.cn; jdybs2@vip.163.com

histone deacetylase that mediates anti-oxidative stress and inflammatory response in many skin diseases[12,13]. Notably, SIRT1 has been directly linked to diabetic skin wound healing. In a diabetic mouse model, upregulation of SIRT1 was associated with increased expression of wound repair-related proteins and growth factors, which collectively enhanced fibroblast activation and vascular regeneration[14]. In addition, activation of SIRT1 also antagonizes H_2O_2 and UV-induced senescence of human fibroblasts[15,16]. These findings confirm that SIRT1 is a key negative regulator of fibroblast senescence, especially in the context of diabetic wounds.

Signal transducer and activator of transcription 3 (STAT3) is a latent cytoplasmic protein that is a key factor in driving fibroblast senescence[17]. It could get phosphorylated and enters the nucleus to initiate downstream gene expression when stimulated by reactive oxygen species (ROS) and other signals[18,19]. Inhibition of STAT3 activity can promote tissue repair in diabetic state[20] and alleviate skin fibroblast senescence[21].The literature indicates that SIRT1 inhibits STAT3 activity by reducing STAT3 Tyr705 phosphorylation[22]. This regulatory effect is particularly important for diabetic tissue repair[23,24].

Acidic fibroblast growth factor (aFGF) is an important mediator in cell growth and differentiation of skin fibroblast[25]. A considerable amount of literature has confirmed that aFGF can modulate the functions of fibroblast to help the wound healing, especially in the diabetic wound. Studies have shown that aFGF can inhibit ROS production in diabetic vascular endothelial cells by activating SIRT1, thereby promoting diabetic wound healing[26]. Based on the preliminary work, we hypothesized that aFGF had the potential to rescue the high glucose (HG) induced fibroblast's senescence phenotype and promote the wound healing of diabetic wound through regulation of SIRT1/STAT3 pathway.

In this study, we observed a significant elevation of SASP in L929 fibroblasts exposed to a HG environment and diabetic wounds. Furthermore, aFGF effectively reversed this via regulation of SIRT1/STAT3 signaling pathway—a process dependent on the modulation of oxidative stress, which was accompanied by the subsequent reduction of ROS, malondialdehyde (MDA), and lactate dehydrogenase (LDH), and the subsequent increase of superoxide dismutase (SOD), catalase (CAT), and glutathione peroxidase (GSH-PX).

Result

aFGF enhances diabetic wound healing and improves the senescent phenotype

Eighteen rats were randomly assigned into 3 groups, with 6 rats per group. Subsequently, 3 rats in each group were sacrificed under isoflurane anesthesia on day 8 and day 14, respectively. (Fig. 1A). Wound healing on the back of the rats was continuously photographed during the experiment (Fig. 1B), and the analysis of wound healing rate (Fig. 1C) showed that HG significantly inhibited the wound healing and aFGF accelerated the wound healing compared to the HG group.

Our observations revealed that on day 8 post-wounding, the markers indicative of aging, specifically p53 and p21, showed an elevated expression in diabetic rats' skin tissues, and fibronectin, one of the major elements of ECM, was in a lower level in diabetic rats' skin tissues. However, aFGF treatment restored the senescence phenotype caused by HG, and the expression of fibronectin (Fig. 1D). Meanwhile, we conducted senescence-related β-galactosidase (SA-β-gal) staining to observe whether aFGF ameliorated local cellular senescence in diabetic rat wounds. The results showed that SA-β-gal staining was significantly more intense in the HG group compared with the normal group, and this intensified staining was notably attenuated after aFGF treatment. (Fig. 1E).

HG stimulation induces L929 fibroblast senescence

HG induction is a common method of modelling diabetic trauma in vitro[27]. To mimic the hyperglycemia in DM, we established a HG-induced L929 fibroblast model to observe that, whether the high level of glucose leads to cellular senescence. Screening for appropriate glucose concentrations by CCK8 experiment, we tested with CTR (11.1 Mm), 25, 50, 75 and 100 mM glucose for 0, 24, 48 and 72 h (Fig. 2A). It was found that 100 mM glucose culture caused the most significant decrease in cell proliferation ability after 72 h, while the proliferative activity of L929 fibroblasts cultured with 25 mM glucose was superior to that of the control group—a phenomenon attributed to short-term metabolic adaptation. Specifically, moderate glucose excess provides additional energy substrates for cell division in the early stage of culture, whereas 11.1 mM glucose is conducive to maintaining the long-term metabolic homeostasis and functional integrity of fibroblasts. This was verified by the EdU assay, which confirmed that cell proliferation was markedly inhibited at the 100 mM glucose concentration (Fig. 2B, C). To assess the effects of high glucose on cellular senescence, we conducted SA-β-gal assays. Clearly, the degree of cellular staining increased with elevating glucose concentration, with the most severe cellular senescence at 100 mM (Fig. 2D). To rule out the influence of osmotic pressure, we used mannitol (100 mM) as an osmotic control to detect cell proliferation and senescence. The results showed that high osmotic pressure inhibited cell proliferation activity, but no obvious senescence phenotype was observed (Supplementary Fig. S1A; Fig. 4).

aFGF promotes the proliferation and migration of HG-induced L929 fibroblasts

To detect the optimal concentration of a for aFGF used on L929 fibroblasts, the CCK8 assay was conducted with different doses (0 μg/mL, 10 μg/mL, 20 μg/mL, 40 μg/mL, and 80 μg/mL). The data illustrated that the cell proliferation-promoting effect of aFGF was strongest at 10 μg/mL, while 20 μg/mL also showed a significant difference compared to the control. After that, the ability of aFGF's proliferation-promoting began to diminish (Fig. 3A). We further verified the effect of aFGF at this concentration in EdU proliferation (Fig. 3B, C) and Transwell migration (Fig. 3D, E) assay. The results are consistent with previous studies that L929 fibroblasts exposed to the high glucose culture environment significantly impaired the proliferation and migration capacities, which are important abilities for wound healing[28–30]. Meanwhile, our results verified that 10 μg/mL of aFGF could salvage the inhibitory effect of high glucose on cell proliferation and migration.

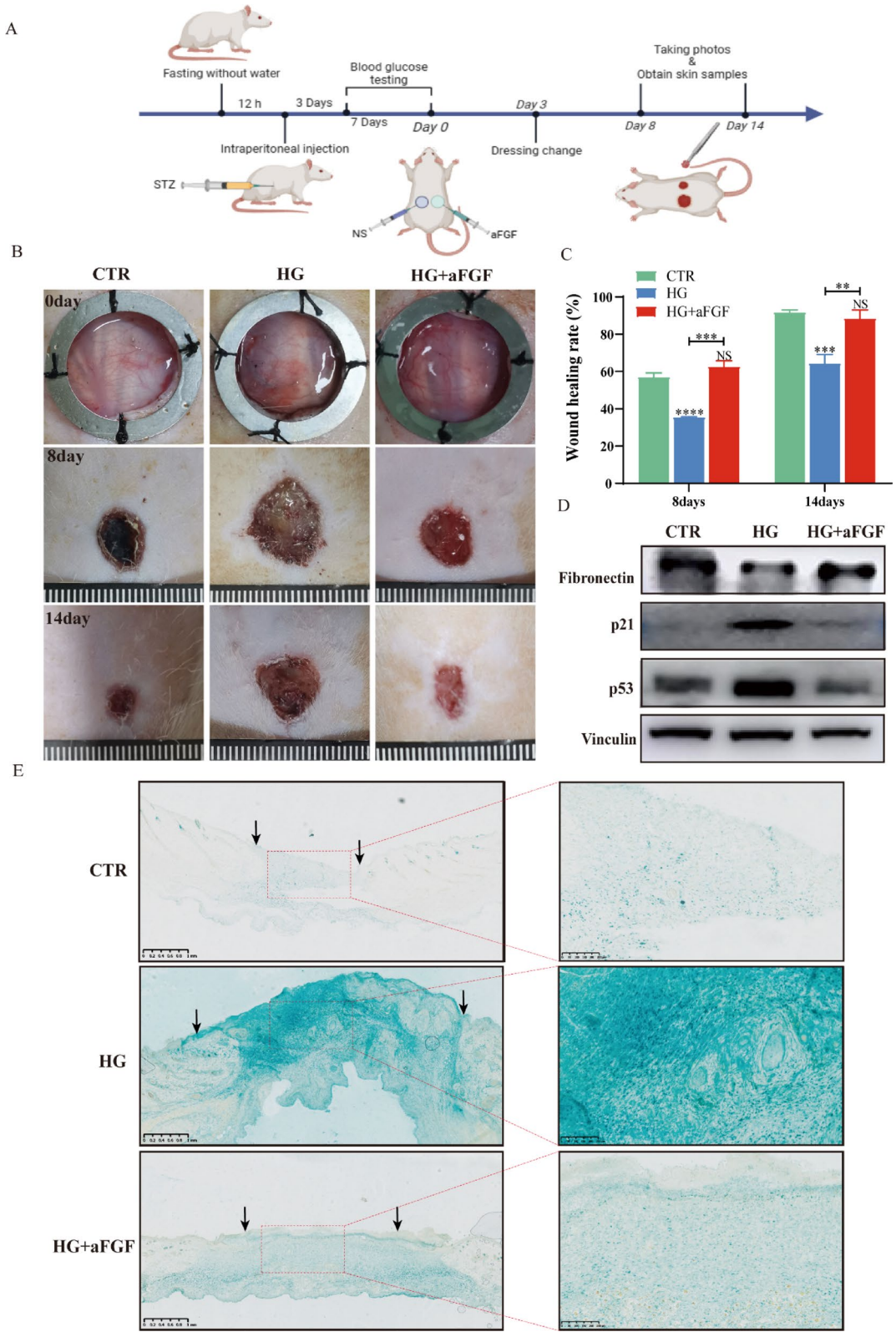

Fig. 1. AFGF promotes wound healing and improves senescent phenotype in diabetic rats. (**A**) Timeline of preparation of diabetic rat wound model. (**B**) Representative photos of full-thickness wounds on the dorsal region of rats. (**C**) Quantitative analysis of wound healing rate on day 8 and 14 after surgery (n = 3). (**D**) Western blot images of p21, p53 and fibronectin expression of diabetic wounds on day 8. (**E**) Representative SA-β-gal staining images of diabetic wounds on day 8 (bar scales = 1 mm or 250 μm; Black arrows represent the edge of wound re-epithelialization.). Results are presented as the mean ± SD. $^{****}P < 0.0001$, $^{***}P < 0.001$, $^{**}P < 0.01$. NS, non-significance vs. the control group.

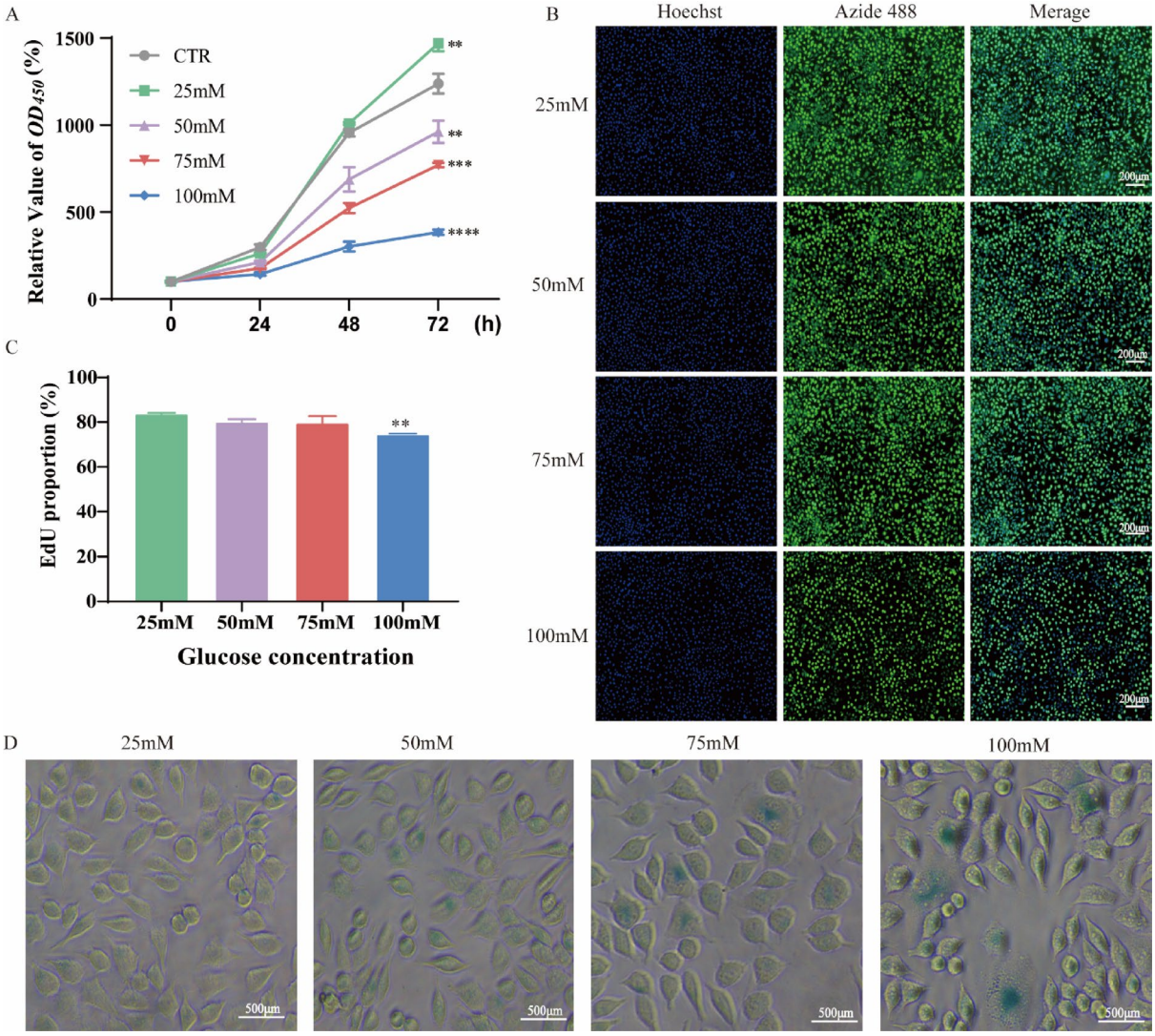

Fig. 2. HG induced L929 fibroblast senescence. (**A**) The relative proliferation activity of L929 induced by different glucose concentrations was measured by CCK-8 (n = 3). (**B**) Representative EDU staining images of L929 after 72 h of exposure to different concentrations of glucose (bar scales = 200 μm). (**C**) Quantitative analysis of EDU staining (n = 3). (**D**) Representative SA-β-gal staining images of L929 after 72 h of exposure to different concentrations of glucose (bar scales = 500 μm). Results are presented as the mean ± SD, $^{****}P < 0.0001$, $^{***}P < 0.001$, $^{**}P < 0.01$, $^{*}P < 0.05$.

aFGF inhibits the senescence of HG-induced L929 fibroblasts

Further, it was revealed that the treatment of aFGF led to the lighter staining of SA-β-gal (Fig. 4A) and a reduction in the expression of senescence biomarkers, specifically the gene (Fig. 4B, C) and protein (Fig. 4D) expression of p53 and p21, which were upregulated in response to 100 mM high glucose. Whereas no significant changes were observed in the mannitol-induced osmotic pressure control group.

It is well-known that cell proliferation is crucial for wound repair. Studies have shown that aFGF can promote cell proliferation in vivo by binding to heparin and fibroblast growth factor receptor (FGFR), thereby exerting an effective endogenous mitogen effect[31,32]. Herein, to rule out the influence of the proliferative effect of aFGF on the results of the anti-senescence study, we used PD173074, a FGFR-specific inhibitor, to block its pro-proliferative effect. The blocking effect was evaluated by immunofluorescence staining of the proliferating cell-associated antigen (Ki67). The results showed that PD173074 (40 nM) could significantly block the pro-proliferative effect of aFGF on L929 cells in the high glucose environment (Supplementary Fig. S1B), but had no significant effect on SA-β-gal (Supplementary Figure S1C). Similarly, PD173074 intervention had no significant effect on the protein expression of p53 after aFGF treatment, while the expression of p21 was increased (Supplementary Fig. S1D). The above results indicate that the ability of aFGF to resist HG-induced cellular senescence can be independent of its pro-proliferative effect; however, the regulation of p21 by aFGF occurs via multiple pathways.

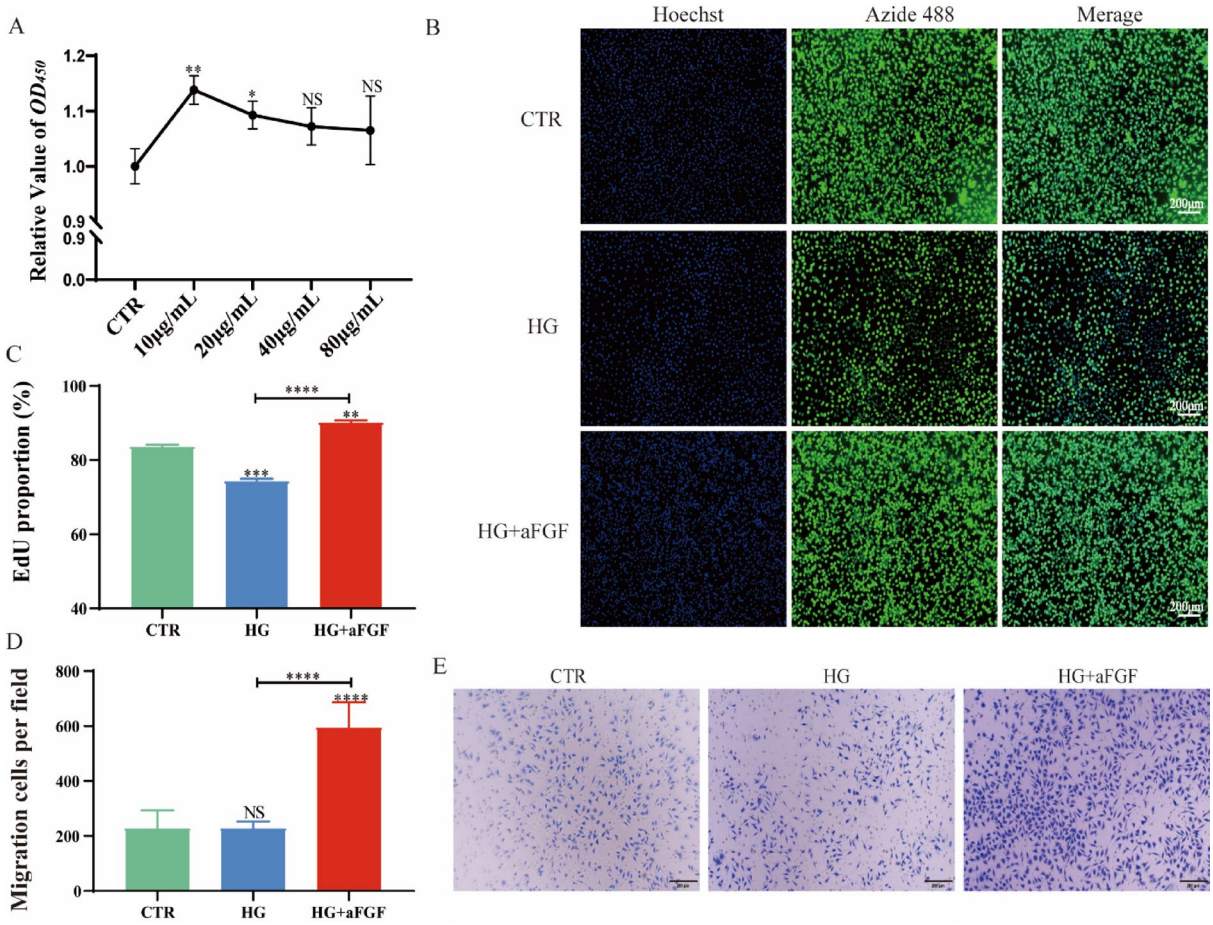

Fig. 3. aFGF enhances the proliferation and migration of HG-induced L929 fibroblasts. (**A**) The relative proliferation of L929 induced by different concentrations of aFGF was measured by CCK-8 (n = 3). (**B**) Representative EDU staining images of L929 after 72 h of exposure to HG or HG and aFGF (bar scales = 200 μm). (**C**) Quantitative analysis of EDU staining (n = 3). (**D**) Quantitative analysis of migrated cells under the transwell chamber in each group (n = 3). (**E**) Representative images of migrated L929 at the outer bottom of the transwell chamber stained by crystal violet in indicated groups. (bar scales = 200 μm). Results are presented as the mean ± SD. $^{****}P < 0.0001$, $^{***}P < 0.001$, $^{**}P < 0.01$, $^{*}P < 0.05$. NS, non-significance vs. the control group.

aFGF ameliorates HG-induced L929 fibroblasts' oxidative stress

It has been reported that excessive oxidative stress plays a major role in delaying wound healing[33]. To further elucidate the mechanisms of aFGF that promote the diabetic wound healing, we tested the oxidative stress levels in cellular level using the classic markers. We observed a pronounced elevation in levels of lactate dehydrogenase (LDH) (Fig. 5A), malondialdehyde (MDA) (Fig. 5B), and reactive oxygen species (ROS) (Fig. 5C) in L929 fibroblasts cultured under high-glucose conditions. Meanwhile, the activities of superoxide dismutase (SOD) (Fig. 5D), catalase (CAT) (Fig. 5E), and glutathione peroxidase (GSH-PX) (Fig. 5F) were significantly reduced. Nevertheless, after the treatment of aFGF, the levels of these oxidative stress related markers involved were decreased, while the levels of the aforementioned antioxidant stress markers were increased.

aFGF inhibits the senescence of HG-induced cells and tissues through the activation of SIRT1/STAT3 pathway

Previous studies have shown that SIRT1 inhibits STAT3 phosphorylation by acting STAT3-Y705[34], and aFGF can resist doxorubicin-induced oxidative stress in cardiomyocytes by activating SIRT1. Therefore, we hypothesized that aFGF might rescue HG-induced cellular senescence by activating SIRT1 pathway. To test our hypothesis, we first examined SIRT1 and STAT3 phosphorylation levels in diabetic wound tissue on the 8th day after injury. The expression level of SIRT1 was higher in the normal rats and lower in the diabetic wound tissues, while the phosphorylation level of STAT3 was the opposite. However, aFGF treatment restored the level of SIRT1 and the phosphorylation level of STAT3 (Fig. 6A).

In order to provide the most direct and significant evidence that aFGF promotes the senescent phenotypic transition in fibroblasts through activation of SIRT1 on STAT3, we first ruled out the impact of aFGF's proliferative effect on SIRT1(Supplementary Fig. S1D). Subsequently, we investigated the effects of EX-527(a

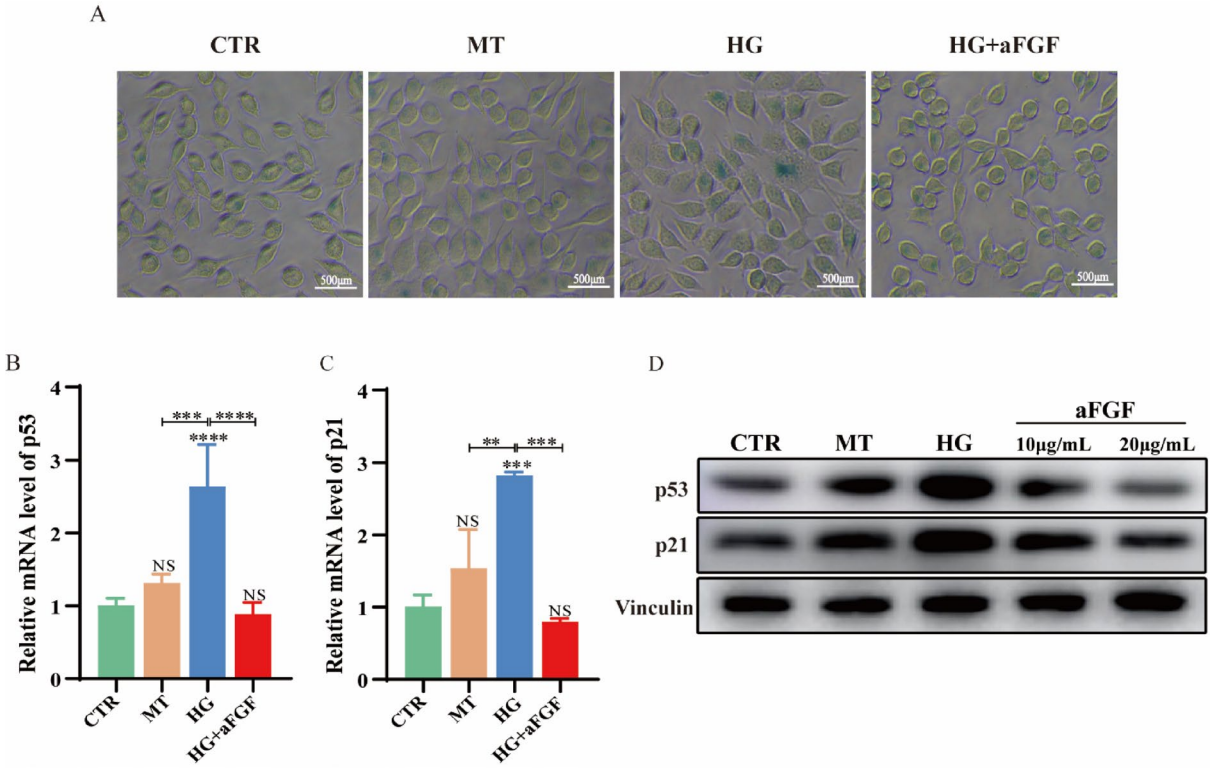

Fig. 4. aFGF inhibits HG-induced L929 fibroblasts' senescence. (**A**) Representative EDU staining images of L929 after 72 h of exposure to HG or HG and aFGF SA- β-gal staining (bar scales = 500 μm). (**B**) The relative mRNA expression level of p53 by RT-qPCR (n = 3). (**C**) The relative mRNA expression level of p21 by RT-qPCR (n = 3). (**D**) Western blot images of p53 and p21 expression of L929 after 72 h of exposure to HG or HG and aFGF. Results are presented as the mean ± SD. ****$P < 0.0001$, ***$P < 0.001$, **$P < 0.01$. NS, non-significance vs. the control group.

SIRT1 inhibitor) on the STAT3 phosphorylation in an aFGF-treated L929 fibroblasts model of high glucose injury. It was showed that the treatment of aFGF led to a lighter staining of SA-β-gal and this kind of effect was reversed by the addition of EX-527 (Fig. 6B). Among which, as the concentration of EX-527 increased (50 nM, 100 nM, 200 nM), the depth of staining increased. Meanwhile, ROS generation increased with the addition of EX-527(200 nM) (Fig. 6C).

aFGF inhibited STAT3 activity via dephosphorylation in HG-induced L929 fibroblasts; however this alternation was reversed by EX-527, as indicated by an increase in phosphorylation at Try 705. Consistent with this trend, the senescence markers (p53 and p21) also exhibited the same expression pattern (Fig. 6D).

To further validate these in vitro observations, we performed in vivo verification using EX-527 in animal models. The results demonstrated that this inhibitor significantly attenuated the promotional effect of aFGF on wound healing in diabetic rats (Fig. 7A, B). Additionally, increased staining intensity of SA-β-gal was observed in wound tissues (Fig. 7C), which further underscores the crucial role of the SIRT1 signaling pathway in this process.

Discussion

SASP factors not only lead to the cell cycle arrest[35], but also cause higher level of inflammatory response[36], slower healing of wounds[37] and so on. An important reason for delayed wound healing in diabetic patients is the persistence of locally cellular senescence in the wound[9]. Normally, fibroblasts perform their functions during the proliferative and tissue remodelling phases of wound healing[30,38], but senescent fibroblasts not only have a reduced ability to proliferate and synthesise ECM, but also release SASP[39], which affects the normal function of neighbouring cells[40]. Our investigation revealed an increase in the expression of senescence markers in the wound of diabetic rats (Fig. 1) and fibroblasts cultivated in an environment with high glucose concentrations (Fig. 2). While, the treatment of aFGF ameliorated the senescence phenotype (Fig. 4). In addition, aFGF expedited the wound healing process in diabetic rats and promoted the deposition of fibronectin in the ECM.

Under normal conditions, inflammatory signals, such as ROS accumulation and increased levels of LDH and MDA, trigger an immune response that results in the elimination of abnormal cells[41]. However, when cells undergo senescence, these clearance systems are disturbed, leading to a strong immune response, sterile inflammation, and a consequent prolongation of the pathological process[42,43]. Thus, these special characteristics exhibited by senescent fibroblasts, including SASP accumulation and excessive oxidative stress, etc., together contribute to the delayed healing of diabetic wounds[44]. In our study, high levels of ROS, LDH and MDA were

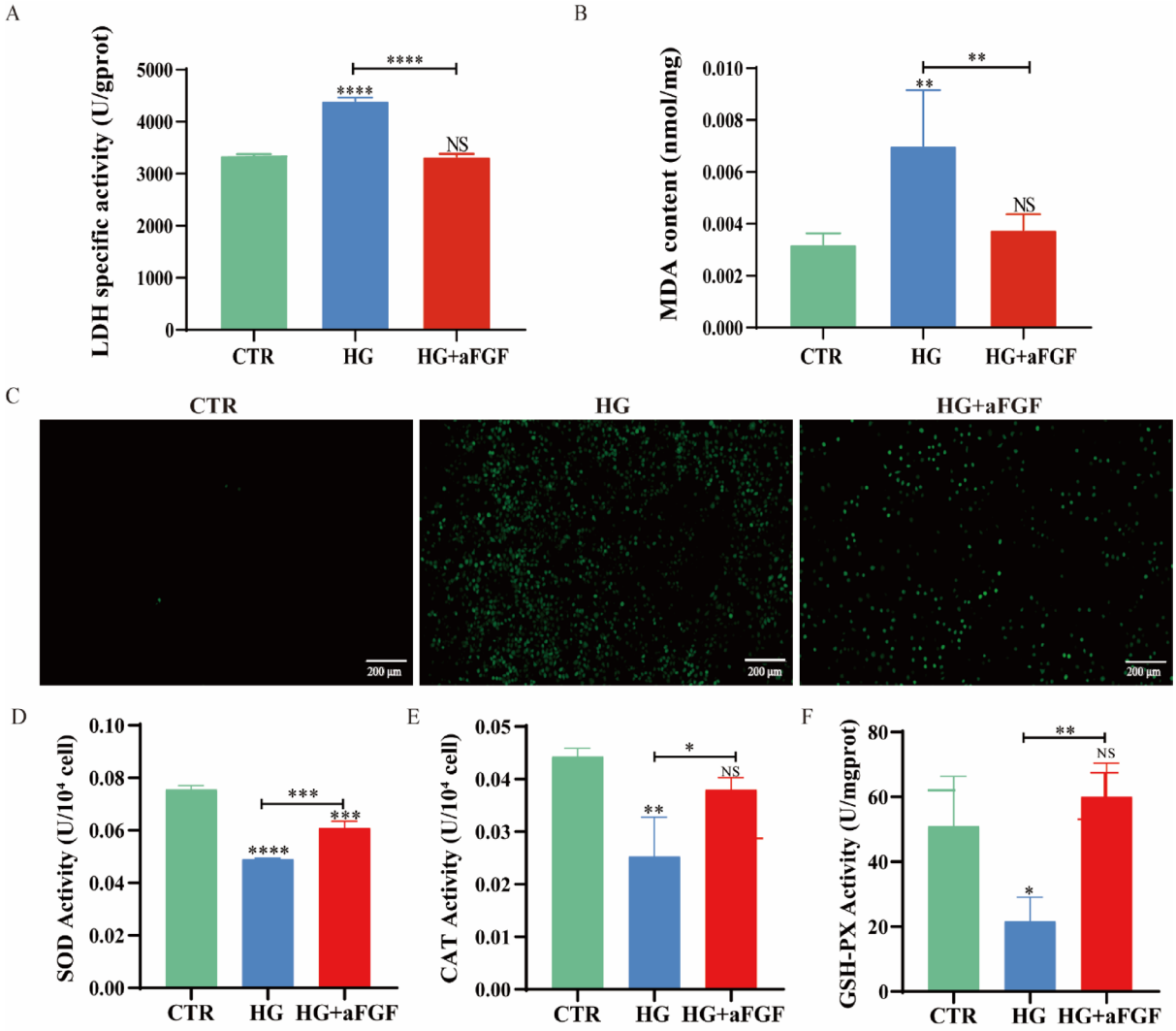

Fig. 5. aFGF ameliorates HG-induced L929 fibroblasts' oxidative stress. (**A**) Activity of LDH in L929 after 72 h of exposure to HG or HG and aFGF (n = 3). (**B**) The content of MDA in L929 after 72 h of exposure to HG or HG and aFGF (n = 3). (**C**) The level of ROS in L929 after 72 h of exposure to HG or HG and aFGF (bar scales = 200 μm). Activity of SOD (D), CAT (**E**) and GSH-PX (**F**) in L929 after 72 h of exposure to HG or HG and aFGF (n = 3). Results are presented as the mean ± SD. $^{****}P < 0.0001$, $^{***}P < 0.001$, $^{**}P < 0.01$, $^{*}P < 0.05$. NS, non-significance vs. the control group.

monitored in both in vitro HG-induced L929 fibroblasts and diabetic rat skin tissues (Fig. 5), consistent with previous studies. It suggests that modulation of the excessive oxidative stress state may simultaneously improve fibroblast senescence in diabetic wounds, thereby promoting wound healing.

Studies have confirmed that aFGF has a strong anti-oxidative stress effect. aFGF can reduce diabetic vascular endothelial dysfunction by inhibiting mitochondrial oxidative stress, and it can also resist adriamycin-induced cardiotoxicity by activating SIRT1[32,45]. Our study also found that aFGF intervention could decrease the levels of LDH, MDA, and ROS in fibroblasts under high-glucose conditions, while increasing the levels of SOD, CAT and GSH-PX (Fig. 5). In addition, we found that SIRT1 synthesis was reduced, STAT3 phosphorylation levels were increased, and protein levels were reversed after aFGF intervention in diabetic rat wound tissue. In vitro experiments (with the SIRT1 inhibitor EX-527) demonstrated that this amelioration is associated with aFGF's regulation of the SIRT1/STAT3 pathway (Fig. 6).

It is noteworthy that aFGF exhibits a robust effect on promoting the proliferation of fibroblasts (Fig. 3). Studies have shown that this effect is mainly mediated by FGFR[31,32], while PD173074 (a specific inhibitor of FGFR) can reverse the pro-proliferative effect of aFGF on tumor cells, adipocytes, and other cell types[46,47]. We acknowledge that the proliferation of fibroblasts during the initial phase of wound healing can advance wound closure, which may introduce some interference with the results of this study. To verify whether crosstalk exists in this process, we used PD173074 to inhibit FGFR and evaluated the status of cell proliferation and senescence. It was found that FGFR inhibition abrogated the pro-proliferative effect of aFGF on fibroblasts (Supplementary Fig. S1B); however, there was no significant change in the anti-senescence effect, as reflected by the accumulation

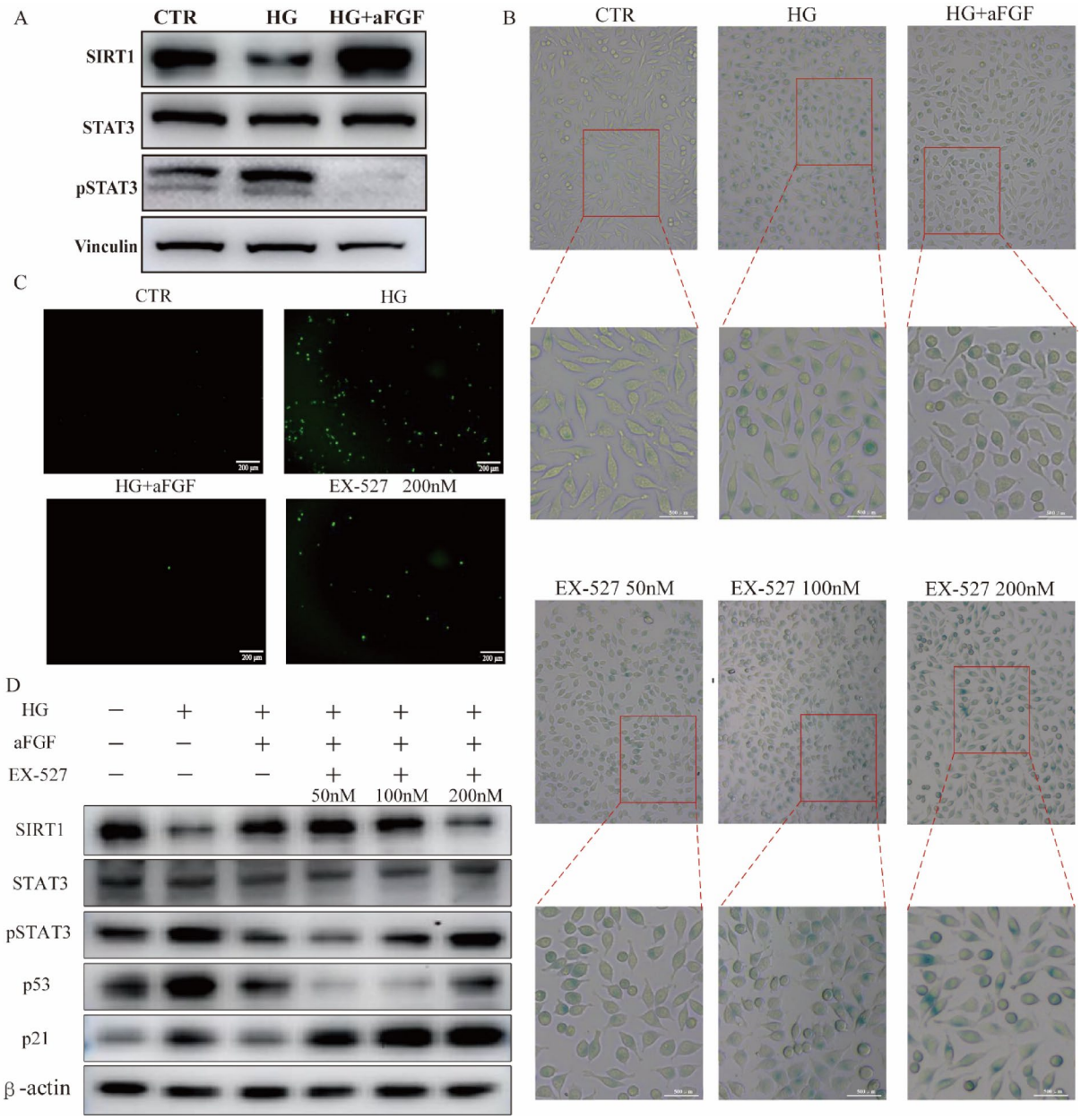

Fig. 6. aFGF inhibits the senescence of HG-induced cells and tissues through the activation of SIRT1/STAT3 pathway. (**A**) Western blot images of SIRT1, STAT3 and pSTAT3 expression of diabetic wounds on day 8. (**B**) Representative images of SA-β-gal staining of L929 treated with EX-527 48 h before staining. (bar scales = 500 μm). (**C**) The level of ROS in L929 treated with EX-527 48 h before detection (bar scales = 200 μm). (**D**) Western blot images of p21, p53, SIRT1, STAT3 and pSTAT3 in L929 treated with EX-527 48 h before extracting the total cellular protein.

levels of SA-β-gal and p53 protein (Supplementary Fig. S1C, D). In contrast, the protein level of p21 increased significantly (Supplementary Fig. S1D). This seems to contradict the well-established conclusion that "p53 is the most well-known upstream regulator of p21". Nevertheless, with the advancement of research, a growing body of evidence has demonstrated that p21 can achieve expression regulation and functional exertion independently of p53 protein[48]. Notably, the promoter region of p21 contains multiple conserved STAT3 binding sites. Phosphorylated STAT3 forms dimers, which bind to the STAT3 binding sites in the p21 promoter, thereby activating p21 expression and inhibiting cell proliferation. This also explains why the expression trend of p21 remains consistent with the phosphorylation level of STAT3 (Fig. 6D).

In conclusion, our results confirm that diabetic wounds exhibit prolonged healing and persistent senescent phenotypes, and aFGF can accelerate diabetic wound healing and alleviate senescent phenotypes both in vivo and in vitro. Additionally, we revealed that aFGF ameliorates senescence by reducing oxidative stress and regulating the SIRT1/STAT3 pathway, suggesting great potential for aFGF in clinical diabetic wound treatment.

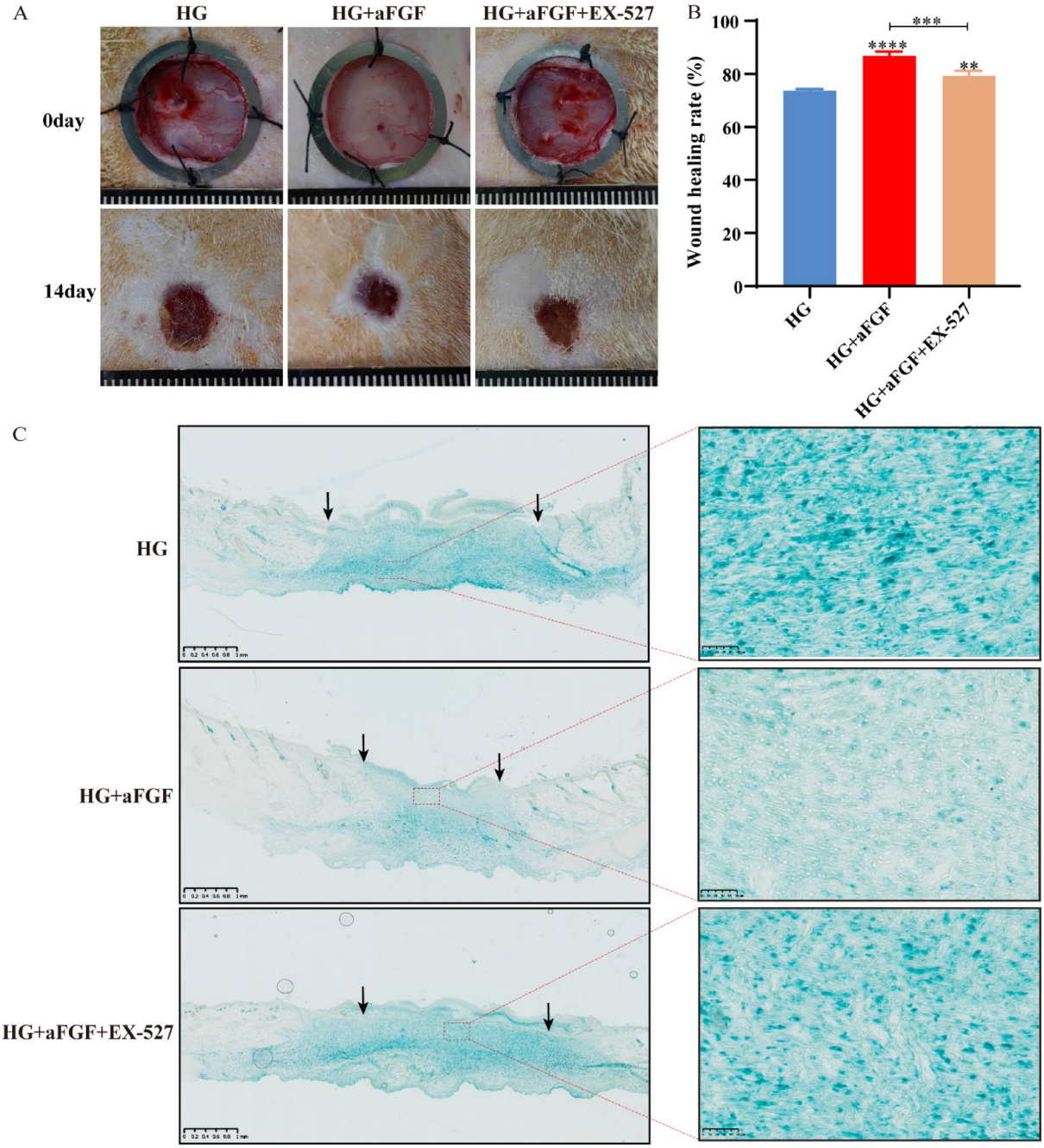

Fig. 7. EX-527 weaken the effect of aFGF on wound healing in diabetic rats. (**A**) Representative photos of full-thickness wounds on the dorsal region of rats. (**B**) Quantitative analysis of wound healing rate on day 14 after surgery (n = 3) (**C**) Representative SA-β-gal staining images of diabetic wounds on day 14 (bar scales = 1 mm or 50 μm; Black arrows represent the edge of wound re-epithelialization.). Results are presented as the mean ± SD. $^{****}P < 0.0001$, $^{***}P < 0.001$, $^{**}P < 0.01$.

However, this study has limitations. First, while aFGF is widely known for promoting cell proliferation, our research focused on its effects on cellular senescence in diabetic wound tissues and did not fully exclude the potential impact of aFGF-induced cell proliferation. Second, chronic diabetic wounds have an extremely complex microenvironment, characterized by hyperglycemia, advanced glycation end-product (AGE) accumulation, hypoxia, insufficient angiogenesis, and chronic inflammation. Our experiments only focused on fibroblast function in a high-glucose microenvironment and failed to fully simulate the complexity of diabetic wounds. Addressing these issues in future studies will deepen understanding of the mechanisms underlying diabetic wound healing.

Methods

Cell culture

Fibroblasts (Clone of mouse connective tissue L929 cell line) were purchased from FuHeng BioLogy (FH0534) and cultured in MEM growth medium (BasalMedia, L510KJ) until the start of experiment. 5 to 7 passage subconfluent cells were used in the experiments. Before starting the experimental procedures, the medium was removed and replaced with Roswell Park Memorial Institute (RPMI) 1640 Medium (M&C GENE TECHNOLOGY, CM10042) supplemented with 1% calf serum (LONSERA, S711-001) for 12 h, then L929 were placed in RPMI 1640 medium consisting of either NG (11.1 mM) or HG (25/50/75/100 mM) in the presence or absence of aFGF (TENRY, P28202306016) for 72 h, mannitol (100 mM: 11.1 mM of glucose + 88.9 mM of D-mannitol) was served as the osmotic control for the HG. The inhibitors PD173074 (KKL MED, KM4912) and EX-527 (MCE, HY-15452) were added to the medium 48 h before cell collection.

Cell viability

Briefly, cells were seeded into 96-well plates at a density of 5×10^3/well with MEM medium. After overnight plating, the medium was removed and replaced with RPMI 1640 medium containing different concentrations of glucose in the presence or absence of aFGF. A Enhanced Cell Counting Kit (CCK)—8 (Elabscience, E-CK-A362) assay was performed to evaluate the cell viability according to the manufacturer's protocol. Each group contained three parallel holes. By incubating the CCK-8 reagent for 2 h, the live cells reacting with the reagent can be detected by a Victor spectrophotometer (Thermo Fisher Scientific, USA).

EdU cell proliferation assay

The proliferation of cells was detected using EdU cell proliferation assay according to the manufacturer's instructions. About 5×10^4 cells were seeded in 6-well plates and maintained for 72 h before the assay. A total of 1 mL EdU (10 μM) reagent (Beyotime, C0071S) was added to each well and incubated for 2 h to label the cells. After three times wash with PBS, cells were fixed in a 4% paraformaldehyde solution (Biosharp, BL539A) for 15 min, permeabilized with 0.3% Triton X-100 (Solarbio, T8200) for another 15 min, and then incubated with the click reaction reagent for 30 min at room temperature in the dark environment. In all, 1 × Hoechst33342 reagent was used to counterstain the nucleus. The result of staining was observed with a fluorescence microscope (OLYMPUS, Japan), and the data were collected by the ImageJ software (1.54p. URL: https://fiji.sc/).

Transwell assay

The transwell assay was used to analyze the migration effect of aFGF toHG-induced L929. 1×10^4 cells were seeded in the upper chamber in MT, HG or HG presence or absence of aFGF, and the bottom chambers contained MEM growth medium containing 10% FBS and 1% P/S. 24 h later, cells were fixed with 4% paraformaldehyde and stained with 0.1% crystal violet, and then the upper surface cells were removed with a cotton swab. The cells of the lower membrane surface were counted under a microscope (OLYMPUS, Japan), and 5 random fields were selected.

SA-β-gal staining

For SA-β-gal staining, L929 cells were treated with MT or HG with or without aFGF, as described in the cell viability and EdU cell proliferation assay. At 72 h, the irradiated cells were fixed in 4% PFA and subjected to SA-β-gal staining with Cell Senescence SA-β-Gal Staining Kit (Beyotime, C0602). After 24 h, the staining solution was aspirated, the six-well plate was washed three times with PBS, a small amount of PBS was added to each well, and the plate was observed using an optical microscope (OLYMPUS, Japan). The senescent cells were stained blue in this experiment. For tissue staining, according to the manufacturer's instructions, we prepared rat skin tissue into frozen sections and performed the same staining protocol.

MDA content detection

MDA levels were measured using the Lipid Peroxidation MDA Assay Kit (Nanjing Jiancheng, A003-1) according to the manufacturer's instructions. Total cellular protein was first extracted using the desired reagents. Then mix 100μL of sample or standard with 100μL of MDA assay reagent-1 in the 5 mL centrifuge tubes. Then, put in 3 mL of reagent-2 and 1 mL of reagent-3. After heating at 95 °C for 40 min and centrifugation at 4000 rpm for 10 min at room temperature, the supernatant is transferred to a 96 well plate. Finally, absorbance was measured at 532 nm at room temperature and the results were calculated from a standard curve.

LDH content detection

Total cellular protein was first extracted using phosphate buffered saline (PBS) with protease inhibitors. Lactate concentrations in L929 fibroblasts were quantified through a Lactate Dehydrogenase assay kit (Elabscience, 1J71NN78KB), following the manufacturer's provided protocol.

Intracellular reactive oxygen species (ROS)

ROS generation was determined using a ROS Assay Kit (Beyotime, S0033S). L929 cells (5×10^4 cells/well) were seeded in 6-well plates and cultured in complete medium. The cells processing method is as described above. The cells were stained with 10 μM DCFH-DA at 37 °C for 20 min and then imaged using a fluorescence microscope.

Antioxidant enzyme activities

The activities of antioxidant enzymes were determined using commercially available assay kits. Briefly, 5×10^6 cells were homogenized in the corresponding extraction buffer provided with the respective assay kit. For the determination of SOD and CAT activities, the homogenates were centrifuged at 8000 g for 10 min, and the

Genes name	Primers sequence (5'→3')
p21	GCAGAATAAAAGGTGCCACAGG
	GACAACGGCACACTTTGCTC
p53	TCCGAAGACTGGATGACTGC
	GATCGTCCATGCAGTGAGGT
GAPDH	AGCCATGTACGTAGCCATCC
	GACTCCATCACAATGCCAGT

Table 1. Primer sequences for quantitative reverse-transcription PCR.

resulting supernatant was used as the enzyme extract for the assays. For the measurement of GSH-PX activity, the enzyme activity was determined directly following cell homogenization. The SOD (BC5165) and CAT (BC0200) activity assay kits were purchased from Beijing Solarbio Science & Technology Co., Ltd., and the GSH-PX assay kit (A005-1) was obtained from the Nanjing Jiancheng Bioengineering Institute.

RNA isolation and quantitative RT-PCR (qRT-PCR)

Total RNA was extracted from L929 by using RNA-Quick Purification Kit (Yishan Biotechnology, RN001). Next, total RNA (500 ng) was reverse transcribed into cDNA by using ABScript III Reverse Transcription Mix for qPCR with gDNA remover Kit (ABclonal, RK20429) and a PCR thermal cycler (Mastercycler gradient, Eppendorf, Germany). The qRT-PCR assay was performed using 2X Universal SYBR Green Fast qPCR Mix (ABclonal, RK21203) and a thermal system (Mastercycler ep realplex, Eppendorf, Germany). The gene expression was quantified as previously described. The mRNA levels of target genes were normalized against those of GAPDH. Gene-specific primer sequences (Tsingke Biotechnology, China) used for qRT-PCR are listed in Table 1.

Immunoblotting analysis

Briefly, 30 μg protein from each sample was resolved by SDS–PAGE on Tris–Glycine gels, and transferred to polyvinylidene fluoride membrane. Membranes were blocked with 5% bovine serum albumin in Tris buffer saline containing 0.1% Tween 20 (TBST) for 1 h, then washed six times for 5 min with TBST and incubated with primary antibodies overnight at 4 ∘C. Membranes were washed six times for 5 min with TBST, incubated in either HRP-goat-anti-rabbit (ZSGB-Bio Cat# ZB-2301, RRID: AB_2747412) secondary antibodies for 1 h at room temperature. Immunoreactive bands were visualized using Pierce ECL plus western blotting substrate (Meilunbio, MA0186). Primary antibodies included: p21 (ABclonal Cat# A2691, RRID: AB_2863018), p53 (ABclonal Cat# A0263, RRID: AB_2757076), SIRT1 (Cell Signaling Technology Cat# 9475, RRID:AB_2617130), STAT3 (Huabio Cat# ET1607-38, RRID:AB_3069762), p-STAT3 (Huabio Cat# ET1603-40, RRID:AB_3069682), Fibronectin (Proteintech Cat# 15613–1-AP, RRID:AB_2105691). The expression of GAPDH (Abways Technology Cat# AB0037, RRID: AB_2891315), β-actin (Abways Technology Cat# AB0035, RRID:AB_2904142) and Vinculin (ABclonal Cat# A2752, RRID:AB_2863020) were used as loading control.

Animal assay

Sprague–Dawley (SD) rats were purchased from Beijing Huafukang Biotechnology Co., Ltd. and housed in the barrier housing facility. All methods were carried out in accordance with relevant guidelines and regulations. All methods are reported in accordance with ARRIVE guidelines (https://arriveguidelines.org). The experimental procedures were approved by the animal laboratory administrative center and the institutional ethics committee of the Second Hospital of Shandong University (Ethics Approval Number: KYLL-2024049). The rats were kept in controlled conditions of temperature (24 ± 2 °C), relative humidity (60 ± 10%) and 12/12 h light/dark cycle (light from 08:00 am to 08:00 pm).

In the experiment validating the effect of aFGF on wound healing in diabetic rats, 18 rats were randomly assigned into three groups (n = 6 per group): (i) normoglycemic control group (CTR group); (ii) streptozotocin (STZ)-induced diabetic rats (HG group); and (iii) STZ-induced diabetic rats + aFGF treatment group (HG + aFGF group). In the EX-527 inhibition experiment, 9 rats were randomly divided into three groups (n = 3 per group): (i) STZ-induced diabetic rats (HG group); (ii) STZ-induced diabetic rats + aFGF treatment group (HG + aFGF group); and (iii) STZ-induced diabetic rats + aFGF + EX-527 treatment group (HG + aFGF + EX-527 group).

Diabetes mellitus was induced in male rats at 8 weeks old, weighing 200 g by intraperitoneal (IP) injection of streptozotocin (STZ, Solarbio, S8050) at the dosage of 30 mg/kg dissolved in 100 mM citrate buffer (pH 4.5) for 3 consecutive days. After one week, blood was collected by rat tail intravenous puncture for measures of glucose using a Glucometer. Rats with a random-blood glucose > 16.7 mmol/L were considered diabetic and were used for the further study.

Full-thickness skin defect wounds were made on the back of rats by surgical operation. Briefly, the rats underwent anesthesia via isoflurane inhalation and subsequently had their back hair removed. Subsequently, a full-thickness skin defect model, measuring 20 mm in diameter, was created on their backs using a tissue scissor. Then, we subcutaneously injected drugs (CTR and HG, saline; aFGF, 3 mg/mL, 200 μL; EX-527, 10 μmol/mL, 100uL) around the wound every 3 days. The radiation-sterilized, anti-shrinkage, and aseptic ring (20 mm OD, 15 mm ID, 1 mm thick) was secured to the perimeter of each skin defect using a 4–0 mousse thread, with four suture points for firm attachment. Post-surgery, the wound was dressed with a 3 M transparent film. Daily observations tracked rat activity and dressing condition, with dressing removal scheduled on day 8.

Wound healing progress was visually assessed and measured on days 0, 8, and 14 post-op, utilizing ImageJ for wound area calculations and healing rate analysis. The wound closure percentage was derived by the formula: [(original wound area—wound area at assessment) / original wound area] × 100%. On days 8 and 14, rats were euthanized with overdose anesthesia, and wound tissue samples were harvested for subsequent use. Each experimental group comprised three rats.

Statistical analysis

The collected data were statistically analyzed with GraphPad Prism version 8 software (GraphPad Software, USA). The results are reported as mean ± SD (standard deviation). The statistical significance of differences was evaluated using either analysis of variance (ANOVA) or standard t-tests. $P < 0.05$, $P < 0.01$, $P < 0.001$, and $P < 0.0001$ indicated statistically significant differences, while NS (denoting non-significant differences) indicated no statistical difference between groups.

Data availability

The data used to support the finding of this study are available from the corresponding author upon request.

Received: 31 October 2024; Accepted: 29 January 2026
Published online: 09 February 2026

References

1. Schwarz, P. E. et al. Global diabetes survey–an annual report on quality of diabetes care. *Diabetes Res. Clin. Pract.* **100**(1), 11–18. https://doi.org/10.1016/j.diabres.2012.11.008 (2013).
2. Powers, J. G., Higham, C., Broussard, K. & Phillips, T. J. Wound healing and treating wounds: Chronic wound care and management. *J. Am. Acad. Dermatol.* **74**(4), 607–626. https://doi.org/10.1016/j.jaad.2015.08.070 (2016).
3. Wilkinson, H. N. & Hardman, M. J. Cellular senescence in acute and chronic wound repair. *Cold Spring Harb. Perspect. Biol.* **14**(11), a041221. https://doi.org/10.1101/cshperspect.a041221 (2022).
4. Wu, D. et al. Downregulation of VEGFA accelerates AGEs-mediated nucleus pulposus degeneration through inhibiting protective mitophagy in high glucose environments. *Int. J. Biol. Macromol.* **262**(Pt 1), 129950. https://doi.org/10.1016/j.ijbiomac.2024.129950 (2024).
5. Berlanga-Acosta, J. A. et al. Cellular senescence as the pathogenic hub of diabetes-related wound chronicity. *Front Endocrinol. (Lausanne)* **11**, 573032. https://doi.org/10.3389/fendo.2020.573032 (2020).
6. Moura, J., Madureira, P., Leal, E. C., Fonseca, A. C. & Carvalho, E. Immune aging in diabetes and its implications in wound healing. *Clin. Immunol.* **200**, 43–54. https://doi.org/10.1016/j.clim.2019.02.002 (2019).
7. Shu, F. et al. Amniotic epithelial cells accelerate diabetic wound healing by protecting keratinocytes and fibroblasts from high-glucose-induced senescence. *Cell Biol. Int.* **46**(5), 755–770. https://doi.org/10.1002/cbin.11771 (2022).
8. Andrade, A. M. et al. Role of senescent cells in cutaneous wound healing. *Biology (Basel).* **11**(12), 1731. https://doi.org/10.3390/biology11121731 (2022).
9. Wilkinson, H. N. et al. Elevated local senescence in diabetic wound healing is linked to pathological repair via CXCR2. *J. Invest. Dermatol.* **139**(5), 1171-1181.e6. https://doi.org/10.1016/j.jid.2019.01.005 (2019).
10. Luo, Y. et al. Adipose mesenchymal stem cell-derived extracellular vesicles regulate PINK1/parkin-mediated mitophagy to repair high glucose-induced dermal fibroblast senescence and promote wound healing in rats with diabetic foot ulcer. *Acta Diabetol.* **62**(7), 1041–1056. https://doi.org/10.1007/s00592-024-02422-x (2025).
11. Garcia-Peterson, L. M. et al. Sirtuins in skin and skin cancers. *Skin Pharmacol. Physiol.* **30**(4), 216–224. https://doi.org/10.1159/000477417 (2017).
12. Wang, Y., Huo, J., Zhang, D., Hu, G. & Zhang, Y. Chemerin/ChemR23 axis triggers an inflammatory response in keratinocytes through ROS-sirt1-NF-κB signaling. *J. Cell Biochem.* **120**(4), 6459–6470. https://doi.org/10.1002/jcb.27936 (2019).
13. Kauppinen, A., Suuronen, T., Ojala, J., Kaarniranta, K. & Salminen, A. Antagonistic crosstalk between NF-κB and SIRT1 in the regulation of inflammation and metabolic disorders. *Cell Signal.* **25**(10), 1939–1948. https://doi.org/10.1016/j.cellsig.2013.06.007 (2013).
14. Bibi, S. et al. Lapachol-induced upregulation of Sirt1/Sirt3 is linked with improved skin wound healing in Alloxan-induced diabetic mice. *Iran J. Pharm. Res.* **20**(3), 419–430. https://doi.org/10.22037/ijpr.2021.112722.13914 (2021).
15. Chung, K. W. et al. Molecular insights into SIRT1 protection against UVB-induced skin fibroblast senescence by suppression of oxidative stress and p53 acetylation. *J. Gerontol. A Biol. Sci. Med. Sci.* **70**(8), 959–968. https://doi.org/10.1093/gerona/glu137 (2015).
16. Lei, Y. et al. Mannan-binding lectin inhibits oxidative stress-induced senescence via the NAD+/Sirt1 pathway. *Int. Immunopharmacol.* **137**, 112468. https://doi.org/10.1016/j.intimp.2024.112468 (2024).
17. Kojima, H., Kunimoto, H., Inoue, T. & Nakajima, K. The STAT3-IGFBP5 axis is critical for IL-6/gp130-induced premature senescence in human fibroblasts. *Cell Cycle* **11**(4), 730–739. https://doi.org/10.4161/cc.11.4.19172 (2012).
18. Sano, S., Chan, K. S. & DiGiovanni, J. Impact of Stat3 activation upon skin biology: A dichotomy of its role between homeostasis and diseases. *J. Dermatol. Sci.* **50**(1), 1–14. https://doi.org/10.1016/j.jdermsci.2007.05.016 (2008).
19. Xu, F., Xu, J., Xiong, X. & Deng, Y. Salidroside inhibits MAPK, NF-κB, and STAT3 pathways in psoriasis-associated oxidative stress via SIRT1 activation. *Redox Rep.* **24**(1), 70–74. https://doi.org/10.1080/13510002.2019.1658377 (2019).
20. Wang, X. et al. The proinflammatory cytokines IL-1β and TNF-α modulate corneal epithelial wound healing through p16Ink4a suppressing STAT3 activity. *J. Cell Physiol.* **235**(12), 10081–10093. https://doi.org/10.1002/jcp.29823 (2020).
21. Hartinger, R., Singh, K., Leverett, J. & Djabali, K. Enhancing cellular homeostasis: Targeted botanical compounds boost cellular health functions in normal and premature aging fibroblasts. *Biomolecules* **14**(10), 1310. https://doi.org/10.3390/biom14101310 (2024).
22. Sestito, R. et al. STAT3-dependent effects of IL-22 in human keratinocytes are counterregulated by sirtuin 1 through a direct inhibition of STAT3 acetylation. *FASEB J.* **25**(3), 916–927. https://doi.org/10.1096/fj.10-172288 (2011).
23. Wen, Y., Wang, J., Duan, M., Li, Q. & Ma, J. SIRT1-mediated regulation of STAT3/SOCS3 inhibits insulin resistance in trophoblast cells and improves gestational diabetes mellitus. *FASEB J.* **39**(9), e70620. https://doi.org/10.1096/fj.202500520R (2025).
24. Sun, H. J. et al. Polysulfide-mediated sulfhydration of SIRT1 prevents diabetic nephropathy by suppressing phosphorylation and acetylation of p65 NF-κB and STAT3. *Redox Biol.* **38**, 101813. https://doi.org/10.1016/j.redox.2020.101813 (2021).
25. He, H. et al. Microneedle patch for transdermal sequential delivery of KGF-2 and aFGF to enhance burn wound therapy. *Small* **20**(34), e2307485. https://doi.org/10.1002/smll.202307485 (2024).

26. Zhang, Y. et al. Acidic fibroblast growth factor inhibits reactive oxygen species-induced epithelial-mesenchymal transdifferentiation in vascular endothelial cells via the miR-155–5p/SIRT1/Nrf2/HO-1 pathway to promote wound healing in diabetic mice. *Burns Trauma*. **12**, take10. https://doi.org/10.1093/burnst/tkae010 (2024).
27. Chen, C., Lin, L. Y., Chen, J. W. & Chang, T. T. CXCL5 suppression recovers neovascularization and accelerates wound healing in diabetes mellitus. *Cardiovasc. Diabetol.* **22**(1), 172. https://doi.org/10.1186/s12933-023-01900-w (2023).
28. Xuan, Y. H. et al. High-glucose inhibits human fibroblast cell migration in wound healing via repression of bFGF-regulating JNK phosphorylation. *PLoS ONE* **9**(9), e108182. https://doi.org/10.1371/journal.pone.0108182 (2014).
29. Bian, X. et al. Regenerative and protective effects of dMSC-sEVs on high-glucose-induced senescent fibroblasts by suppressing RAGE pathway and activating Smad pathway. *Stem Cell Res. Ther.* **11**(1), 166. https://doi.org/10.1186/s13287-020-01681-z (2020).
30. Talbott, H. E., Mascharak, S., Griffin, M., Wan, D. C. & Longaker, M. T. Wound healing, fibroblast heterogeneity, and fibrosis. *Cell Stem Cell* **29**(8), 1161–1180. https://doi.org/10.1016/j.stem.2022.07.006 (2022).
31. Belov, A. A. & Mohammadi, M. Molecular mechanisms of fibroblast growth factor signaling in physiology and pathology. *Cold Spring Harb. Perspect. Biol.* **5**(6), a015958. https://doi.org/10.1101/cshperspect.a015958 (2013).
32. Xiao, M. et al. A new FGF1 variant protects against adriamycin-induced cardiotoxicity via modulating p53 activity. *Redox Biol.* **49**, 102219. https://doi.org/10.1016/j.redox.2021.102219 (2022).
33. Dehdashtian, E. et al. Diabetic retinopathy pathogenesis and the ameliorating effects of melatonin; involvement of autophagy, inflammation and oxidative stress. *Life Sci.* **193**, 20–33. https://doi.org/10.1016/j.lfs.2017.12.001 (2018).
34. Xu, J., Liu, X., Zhao, F., Zhang, Y. & Wang, Z. HIF1α overexpression enhances diabetic wound closure in high glucose and low oxygen conditions by promoting adipose-derived stem cell paracrine function and survival. *Stem Cell Res. Ther.* **11**(1), 148. https://doi.org/10.1186/s13287-020-01654-2 (2020).
35. Acosta, J. C. et al. Chemokine signaling via the CXCR2 receptor reinforces senescence. *Cell* **133**(6), 1006–1018. https://doi.org/10.1016/j.cell.2008.03.038 (2008).
36. Acosta, J. C. et al. A complex secretory program orchestrated by the inflammasome controls paracrine senescence. *Nat. Cell Biol.* **15**(8), 978–990. https://doi.org/10.1038/ncb2784 (2013).
37. Ma, Z. et al. PDK4 rescues high-glucose-induced senescent fibroblasts and promotes diabetic wound healing through enhancing glycolysis and regulating YAP and JNK pathway. *Cell Death Discov.* **9**(1), 424. https://doi.org/10.1038/s41420-023-01725-2 (2023).
38. Driskell, R. R. et al. Distinct fibroblast lineages determine dermal architecture in skin development and repair. *Nature* **504**(7479), 277–281. https://doi.org/10.1038/nature12783 (2013).
39. Zhao, R. et al. Precise diabetic wound therapy: PLS nanospheres eliminate senescent cells via DPP4 targeting and PARP1 activation. *Adv. Sci. (Weinh).* **9**(1), e2104128. https://doi.org/10.1002/advs.202104128 (2022).
40. Coppé, J. P. et al. Senescence-associated secretory phenotypes reveal cell-nonautonomous functions of oncogenic RAS and the p53 tumor suppressor. *PLoS Biol.* **6**(12), 2853–2868. https://doi.org/10.1371/journal.pbio.0060301 (2008).
41. Parrinello, S. et al. Oxygen sensitivity severely limits the replicative lifespan of murine fibroblasts. *Nat. Cell Biol.* **5**(8), 741–747. https://doi.org/10.1038/ncb1024 (2003).
42. Duan, J., Duan, J., Zhang, Z. & Tong, T. Irreversible cellular senescence induced by prolonged exposure to H2O2 involves DNA-damage-and-repair genes and telomere shortening. *Int. J. Biochem. Cell Biol.* **37**(7), 1407–1420. https://doi.org/10.1016/j.biocel.2005.01.010 (2005).
43. Davalli, P., Mitic, T., Caporali, A., Lauriola, A. & D'Arca, D. ROS, cell senescence, and novel molecular mechanisms in aging and age-related diseases. *Oxid Med. Cell Longev.* https://doi.org/10.1155/2016/3565127 (2016).
44. Wei, X. et al. Defective NCOA4-dependent ferroptosis in senescent fibroblasts retards diabetic wound healing. *Cell Death Discov.* **9**(1), 138. https://doi.org/10.1038/s41420-023-01437-7 (2023).
45. Sun, J. et al. aFGF alleviates diabetic endothelial dysfunction by decreasing oxidative stress via Wnt/β-catenin-mediated upregulation of HXK2. *Redox Biol.* **39**, 101811. https://doi.org/10.1016/j.redox.2020.101811 (2021).
46. Widberg, C. H. et al. Fibroblast growth factor receptor 1 is a key regulator of early adipogenic events in human preadipocytes. *Am. J. Physiol. Endocrinol. Metab.* **296**(1), E121–E131. https://doi.org/10.1152/ajpendo.90602.2008 (2009).
47. Ye, T. et al. Inhibition of FGFR signaling by PD173074 improves antitumor immunity and impairs breast cancer metastasis. *Breast Cancer Res. Treat.* **143**(3), 435–446. https://doi.org/10.1007/s10549-013-2829-y (2014).
48. Phalke, S. et al. p53-Independent regulation of p21Waf1/Cip1 expression and senescence by PRMT6. *Nucleic Acids Res.* **40**(19), 9534–9542. https://doi.org/10.1093/nar/gks858 (2012).

Author contributions

Data curation, Xiaoyang Wang, Meiqi Lu, Shanshan Jia, Jingjuan Zhang, Xiao Wang, Yongjun Qi and Nian Shi; Funding acquisition, Duyin Jiang; Methodology, Xiaoyang Wang; Project administration, Duyin Jiang; Resources, Xiao Wang and Yongjun Qi; Supervision, Jixun Zhang and Duyin Jiang; Validation, Meiqi Lu; Visualization, Xiaoyang Wang and Ya Jiao; Writing – original draft, Xiaoyang Wang, Meiqi Lu; Writing – review & editing, Xiaoyang Wang, Jie Zhao and Xiaochuan Wang.

Funding

This work was supported by the National Natural Science Foundation of China (82202454, 81873934), Wang Zhengguo Foundation for Traumatic Medicine (growth factor rejuvenation project, SZYZ-TR-09), Science and Technology Development Projects of Shandong Province (2015GSF118041), the Youth Fund from Natural Science Foundation of Shandong Province (ZR2020QH168), Jinan Science and Technology Plan Project (202225065).

Declarations

Competing interests

The authors declare no competing interests.

Additional information

Supplementary Information The online version contains supplementary material available at https://doi.org/10.1038/s41598-026-38480-0.

Correspondence and requests for materials should be addressed to J.Z., X.W., J.Z. or D.J.